7-1-2023

Impact of microplastics on organic fouling of hollow fiber membranes

Sahar Ghasemi

Bin Yan

Masoumeh Zargar
Edith Cowan University

Nicholas N.A. Ling

Einar O. Fridjonsson

See next page for additional authors

10.1016/j.cej.2023.143320
Ghasemi, S., Yan, B., Zargar, M., Ling, N. N., Fridjonsson, E. O., & Johns, M. L. (2023). Impact of microplastics on organic fouling of hollow fiber membranes. Chemical Engineering Journal, 467, article 143320. https://doi.org/10.1016/j.cej.2023.143320

Chemical Engineering Journal 467 (2023) 143320

Contents lists available at ScienceDirect

Chemical Engineering Journal

journal homepage: www.elsevier.com/locate/cej

Impact of microplastics on organic fouling of hollow fiber membranes

Sahar Ghasemi [a], Bin Yan [a], Masoumeh Zargar [b], Nicholas N.A. Ling [a], Einar O. Fridjonsson [a], Michael L. Johns [a,*]

[a] Department of Chemical Engineering, School of Engineering, University of Western Australia, Crawley, WA 6009, Australia
[b] School of Engineering, Edith Cowan University, 270 Joondalup Drive, Joondalup, WA 6027, Australia

ARTICLE INFO

Keywords:
Hollow fiber (HF) membrane
Magnetic resonance imaging (MRI)
Velocity mapping
Microplastics (MPs)
Fouling
Alginate gel

ABSTRACT

Given the potential hazards of microplastics (MPs), it is desirable to efficiently remove them during wastewater treatment processes. To this end, ultrafiltration (UF) membranes can significantly increase the removal of MPs, however the fouling of such membrane modules can also be impacted by the presence of MPs. Magnetic Resonance Imaging (MRI) was used here to non-invasively quantify the effect of polyethylene (PE) MPs accumulation in a 3D UF hollow fiber (HF) membrane module containing 400 fibers, via direct non-invasive velocity imaging of the flow distribution between individual fibers during module operation. The co-effect of MPs and alginate (a common organic model foulant mimicking extracellular polymeric substances (EPS)) on fouling of the HF module was then explored. Flow was initially equally distributed with fouling causing flow in particular fibers to be significantly reduced. Fouling with MPs resulted in minimal flow distribution disruption and was easily remediated hydraulically, in contrast alginate fouling required chemical cleaning in order to fully restore homogeneous flow distribution between the fibers. The presence of both MPs and alginate resulted in a more heterogeneous disruption of the fibre flow distribution due to fouling and resulted in much more effective hydraulic cleaning of the module.

1. Introduction

Microplastics (MPs) are prevalent in atmospheric, aquatic and terrestrial environments; due to their small size (1 μm–5 mm) and their density (0.92–0.97 g/cm^3), they are easily suspended in water and can be readily transported by wind or water flow [1]. Growth in the world's plastic production, poor waste management of plastics and their comparative lack of biodegradability have accordingly led to the ubiquitous presence and persistence of MPs in aquatic ecosystems [2]. There is significant research showing that MPs are found in significant quantities in human foods such as dairy milk products, beverages, condiments, meat, seafood, salt and vegetables [3–5]. Research conducted on tap water, bottled water and fresh water in different parts of the world, such as Canada [6], Germany [7,8], China [9] and the Czech Republic [10] has revealed the presence of significant amounts of MPs in drinking water.

MPs can induce toxic effects on biota and human health through several potential mechanisms. The toxicity could be directly caused by the polymer materials [3], the additives that are used to improve the plastic properties or the attachment of pathogens and toxic materials to the MPs structure via exposure to contaminated media [11,12]. MPs can also function as carriers of persistent organic pollutants by adsorption to their typically hydrophobic surfaces [13]. Any adverse effects on human health are likely to be accentuated for smaller MPs on account of their comparatively larger surface-to-volume ratio [14]. A significant source of MPs in the environment is the discharge of effluent from wastewater treatment plants [15,16]. Although up to 98.5% of MPs are removed in primary, secondary and advanced tertiary treatment steps, it is estimated that up to 4.5 million MP particles are released to the environment on a daily basis due to the discharge of comparatively large volumes of effluent into the aquatic environment [17]. MPs >500 μm generally accounted for more than 90% of total MPs in the effluents of such wastewater treatment plants, whilst in some effluent samples, MPs less than 100 μm constituted approximately 60% of all discharged MPs [11]. Ultrafiltration (UF) membrane modules used in wastewater treatment plants can increase MP removal by up to 99.9% [18]. Fouling and thus costly maintenance requirements, however, often limit the application of such UF membrane modules [15]. MPs can potentially increase (or decrease) fouling of all types in such membrane modules during wastewater treatment processes on account of their propensity to

* Corresponding author.
E-mail address: michael.johns@uwa.edu.au (M.L. Johns).

https://doi.org/10.1016/j.cej.2023.143320
Received 25 January 2023; Received in revised form 12 April 2023; Accepted 1 May 2023
Available online 9 May 2023

physically or chemically interact with both the membrane and other foulant materials, adsorb and deposit on the membrane surface or in their pores [15].

The potential effects of MPs on membrane fouling depend on various factors, such as the size, shape and chemical composition of the MPs, the type of membrane, and the feed solution [15]. Smaller MPs tend to obstruct pores, increasing filtration resistance [19], whereas larger MPs can form macro-voids between the membrane and deposits, resulting in a more porous cake layer structure that can alleviate fouling [20]. Additionally and of significant importance, the chemical composition and physicochemical properties of MPs, which may change with aging, can influence their interaction with the membrane surface and other foulants present in the feed solution [15].

A synergistic effect between MPs and other foulants has been observed in certain literature [19,21–24] to lead to more pronounced membrane fouling. Conversely, in other literature [18,20,25–27], MPs have been observed to mitigate other fouling by inducing a more heterogeneous and porous fouling structure, resulting in both comparatively less flux decline and a looser cake layer that is easier to dislodge. Other literature, in turn (e.g. [28]), has reported negligible influence from MPs on fouling. The key features and outcomes of these recent studies are extensively detailed in Table S1 in the Supplementary Information. Consistent across all these studies is the use of invasive measurements, extensive sample preparation prior to analysis or simple bulk measurements (e.g. transmembrane pressure drop). None provide non-invasive determination at the fiber-scale of fouling development in operating three-dimensional and opaque modules, such insight is unique to our work.

In this work, MRI velocity mapping was applied to non-invasively explore any synergistic effects of combined MPs and alginate gel (a common biological foulant simulant) fouling inside an opaque hollow fiber (HF) membrane module containing 400 fibers. Due to their numerous advantages over alternative membrane configurations, such as a high packing density, a larger membrane area per unit volume, reduced fouling caused by the shear stress generated by the tangential flow and hence enhanced productivity, hollow fiber membranes have become the preferred choice for a broad range of industrial water treatment applications [29,30]. Polyethylene (PE) was selected as it is a predominant MP polymer type found in wastewater treatment plants and is widely utilised in the production of plastic bags, food packaging material, bottles, containers, toys and personal care products (e.g., facial cleansers, shampoos) [1,31]. The real-time build-up of fouling and resultant flow redistribution between 400 fibers, as well as subsequent hydraulic and chemical cleaning, were thus directly quantified and explored. Hydraulic cleaning was performed by backwashing the membrane with deionised (DI) water, while chemical cleaning was conducted by soaking the fibers in an alkaline solution.

2. Background

2.1. Combined membrane fouling involving microplastics

MP particulate fouling of membrane systems typically progresses from pore clogging to cake layer deposition [32]. This progression (and accompanying membrane flux decline) was observed for PE nanoplastics and MPs in a UF process using a polysulfone membrane [32]. Extracellular polymeric substances (EPS) such as polysaccharides and proteins are also major foulants in wastewater treatment processes that are commonly formed by microorganisms in water [33]. Sodium alginate is a hydrophilic microbial polysaccharide that is commonly used as a model compound in laboratory research to simulate EPS behaviour during the filtration process [33]. In the presence of divalent cations such as Ca^{2+}, the calcium ion binds cooperatively to the carboxylic group of alginates and forms a structured gel known as an “egg-box” shaped gel network, which adversely affects membrane performance [34,35].

There is a limited body of literature concerning any synergistic effects between MPs and alginates or EPS in terms of membrane fouling. Xiong *et al.* [22] showed that MPs can increase the production of EPS by stimulating microbial activity. A dense and compact biofouling layer was subsequently observed during the process of ultrafiltration. Li *et al.* [24] reported synergistic effects between MPs and natural organic matter during membrane fouling; larger transmembrane pressure (TMP) and more severe fouling were observed when MPs were added to the existing organic matter in water. Yogarathinam *et al.* [36] also reported that the co-existence of organic foulants (humic acid and sodium alginate) and MPs caused a higher flux decline than individual MPs during the microfiltration process using a ceramic HF membrane. The synergistic effect of MPs (0.5–5 μm) and humic acid on the fouling of the forward osmosis (FO) membrane was investigated by Golgoli *et al.* [21]. In this case, the combined effect of MPs and humic acid resulted in a higher flux decline compared to MPs and HA alone. A complete flux recovery was achieved by hydraulic cleaning for all fouled membranes due to the lack of hydraulic pressure in the FO process. The co-effect of MPs and humic acid on the fouling of a flat sheet polyethersulfone membrane was investigated by Chen *et al.* [25]. In contrast to previous studies, it was observed that the presence of MPs in pre-coagulation systems, with the application of a suitable coagulant, was beneficial in optimizing the fouling structure, obtaining stable flux and reducing fouling. Additionally, *Ma et al.* [27] reported that the fouling layer structure formed by the combined Fe-based coagulant and MPs was more heterogeneous with larger porosity than the cake layer formed by Fe-based coagulant alone (without MPs). Maliwan *et al.* [18] investigated the combined impact of MPs and EPS on the fouling of a flat sheet polyvinylidene fluoride membrane bioreactor. The findings revealed that the addition of MPs resulted in a reduction in membrane fouling by serving as a scouring material. Markazi *et al.* [20] studied the synergistic effect of MPs and bovine serum albumin (BSA) on the fouling of a flat sheet polyethersulfone membrane. The results demonstrated that MPs interfered with BSA adsorption onto the membrane surface, resulting in a less compact cake layer structure and reduced fouling. Wang *et al.* [26] investigated the fouling behaviour of combined MPs and EPS in a flat sheet cellulose triacetate forward osmosis (FO) membrane. The findings indicated that MPs decreased the membrane fouling caused by EPS by creating a loosely arranged and porous fouling layer with some cracks. This, in turn, made it easier to remove the fouling layer in a cleaning process.

This limited range of studies considered only the effect on overall membrane performance in typically flat-sheet module arrangements; the microstructural characterisation of the resultant foulant was not explored, nor was the effect of combined fouling on various fouled membrane remediation strategies. In our previous study, the fouling mechanism of alginate gel in a HF membrane module and its effect on the flow distribution between fibers were studied using magnetic resonance imaging (MRI) [35]. Here we apply MRI velocity mapping to non-invasively and systematically investigate the combined effect of alginate gel and MPs on the fouling (and subsequent cleaning) in operating HF membrane modules. To the best of our knowledge, neither the effect of MPs nor the combined effect of MPs and alginate gel on membrane fouling has been studied non-invasively in realistic 3D membrane module geometries using MRI.

2.2. NMR/MRI studies of membrane fouling

There is a significant body of literature detailing the application of both nuclear magnetic resonance (NMR) and magnetic resonance imaging (MRI) for the non-invasive exploration of fouling development in membrane module systems, as well as their subsequent remediation (e.g. [37,38]). Although membrane characterization techniques such as SEM, TEM and FTIR provide important information on the morphology and chemical constituents of the membrane foulants, these methods are destructive in this context and cannot be applied for in situ monitoring

of fouling formation [39]. MRI has been used for both non-invasive structural and velocity imaging in order to detect fouling inside different membrane configurations such as HF membrane modules [35], spiral wound membrane modules [40] and flat sheet membranes [41]. Several studies have used MRI velocity measurement to study the fouling formation of sodium alginate in HF membrane modules at different concentrations of Ca^{2+} [42–44]. Schork *et al.* [45] utilised MRI to investigate the response of membrane fouling in a ceramic HF membrane to various cleaning treatments. Using MRI, it was observed how persistent some fouling structures were, these were only partly detached from the membrane by backwashing. Compressed sensing MRI was employed by Simkins *et al.* [46] to rapidly and non-invasively visualise biofouling development inside a polysulfone multichannel HF module containing seven channels, each with an inner diameter of 0.9 mm. Filtration was conducted in dead-end operation mode, and in situ imaging was conducted during the filtration process. In this method, reducing the NMR signal relaxation times enabled faster imaging during filtration, which made it feasible to investigate the spatiotemporal behaviour of biofilm deposition and dissociation during filtration and cleaning processes, respectively. The effect of membrane structure on performance can also be studied by MRI. For example, Wiese *et al.* [47] changed the filtration operational conditions by improving the membrane surface morphology in order to mitigate membrane fouling. MRI velocity mapping measurement was used to visualise the flow-field and flux distribution inside the tubular membrane before and after the change in the membrane. Yan *et al.* [35,55] demonstrated the use of benchtop MRI velocity mapping to characterize the structure and performance of a closely packed UF HF membrane module containing 400 fibers. MRI was successfully applied to resolve the location, size and velocity distribution inside each individual fiber of the operating module as a function of alginate gel fouling extent and remediation.

3. Material and methodology

3.1. Materials and alginate gel preparation

PE powder (with an average particle size of 125 μm and a density of 0.94 g/mL) was purchased from Sigma Aldrich. A commercial sodium alginate powder was obtained from FMC Manugel GMB. Calcium chloride ($CaCl_2$, 93% purity) and sodium chloride (NaCl, 99.9% purity) were bought from Thermo Fisher Scientific. Sodium Hydroxide (NaOH, 98% purity) was purchased from Chem-Supply (CSA Scientific). DI water was used in all experiments to avoid contamination from other sources.

The alginate solution (0.2 wt%) was prepared by dissolving sodium alginate powder in DI water at a concentration of 2000 mg/L and then mixing it with Ca^{2+} ($CaCl_2$) and Na^+ (NaCl) at concentrations of 700 and 1000 mg/L, respectively. The relative volume of $CaCl_2$/NaCl solution to the alginate solution was 2:3 (v/v). Na^+ was thus used as an initiator for alginate–calcium bonding.

3.2. Ultrafiltration membrane modules

Polysulfone UF HF modules, developed by Asahi Kasei Corporation (SIP-1023 and SIP-1013), with molecular weight cut off (MWCO) of 6000 Da, were used in this work. The modules comprise 400 fibers with an inner diameter of 0.8 mm, an outer diameter of 1.2–1.4 mm and a length of 205 mm. The housing is a polysulfone cylindrical chamber with an inner diameter of 36 mm, an outer diameter of 42 mm and a length of 347 mm. The feed side and permeate side volumes were 90 and 130 mL, respectively. The detailed parameters of the membrane module are presented in Table S2 in the Supplementary Information. The modules were operated under an inside-out flow configuration, leading to fouling development on the inner surface of the fibers. The bottom shell-side port of the modules was sealed as this section was placed inside the magnet bore of the NMR spectrometer, while permeate was produced from the top lateral port. Fig. 1(a) shows a side view of the module. Fig. 1(b) shows the top of the membrane module with the cap removed prior to fouling. For reference, Fig. 1(c) shows a sample image of this fiber bundle following the introduction of alginate gel to the feed stream; residual foulant is evident in the vicinity of the fiber entrances.

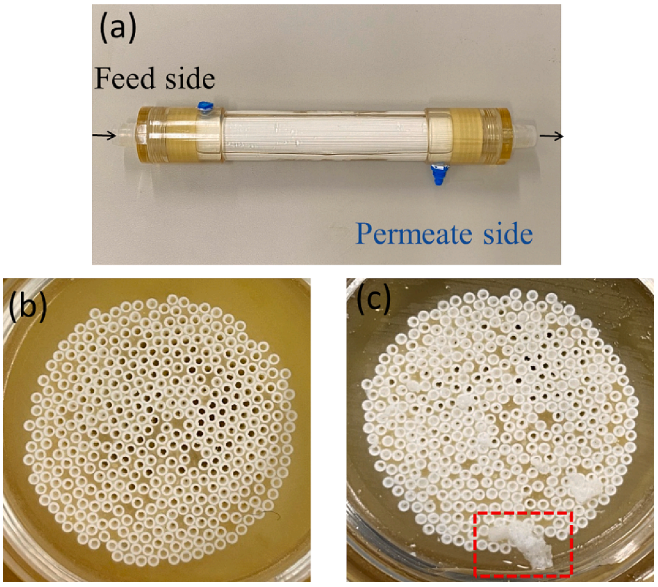

Fig. 1. The UF membrane module (a) from the side and from the top (entry cap removed) for (b) the clean membrane, and (c) a sample image of a fouled membrane with alginate gel visually evident (partial accumulation of the foulant on the fiber entrance is shown in the red dashed box). (For interpretation of the references to colour in this figure legend, the reader is referred to the web version of this article.)

3.3. MRI instrument and imaging protocol

All MRI measurements were performed on a bench-top Oxford MARAN DRX NMR Rock Core Analyser (RCA) with a 0.3 T permanent magnet and ^1H resonance frequency of 12.9 MHz (Fig. 2). The NMR

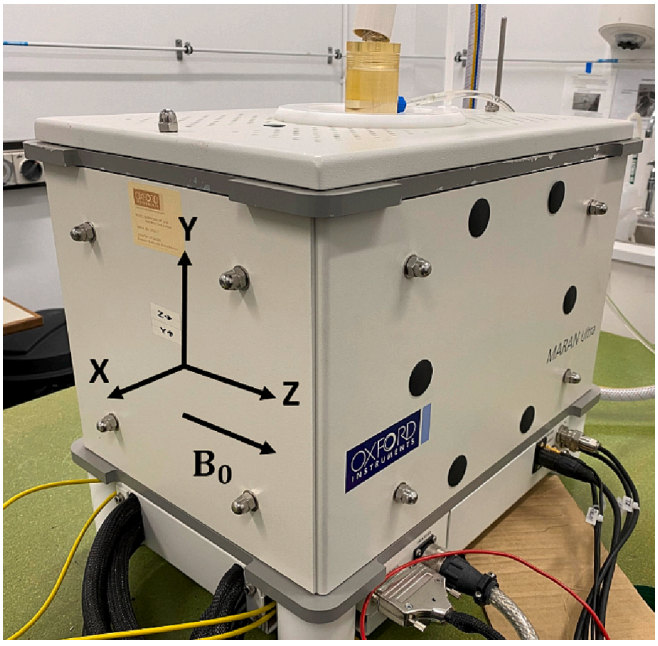

Fig. 2. Low-field benchtop MRI instrument with a UF HF membrane module placed inside the magnet bore. The magnetic field (B_0) is in the z-axis direction.

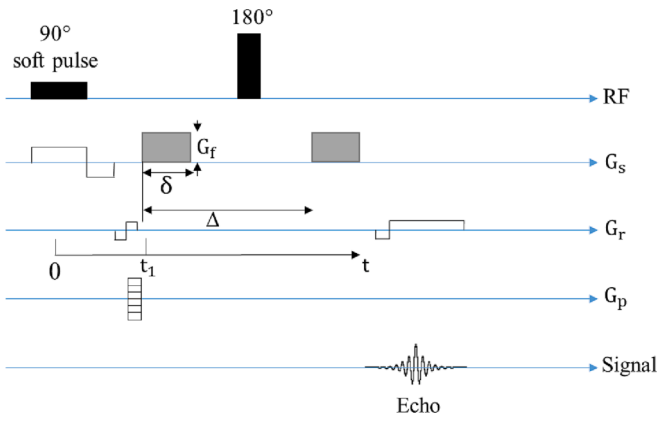

Fig. 3. Pulse sequence used for the flow velocity measurements in a 2D plane (adaptation of the Flow90 pulse sequence as provided by Oxford Instruments) with velocity-encoding gradient amplitude G_f, pulse duration $\delta = 2$ ms, gradient pulse spacing $\Delta = 16$ ms, echo time, $T_E = 38$ ms and a repetition time $T_R = 4$ s.

Table 1
Pulse sequence parameters used in the flow velocity measurements.

MRI parameters	Value
T_R	4 s
T_E	38 ms
In plane resolution Δx, Δz	146 μm
Slice thickness Δy	30 mm
Flow encode gradient duration (δ)	2 ms
Flow encode gradient separation (Δ)	16 ms

signal was obtained exclusively from water molecules. The magnet cylindrical access bore has dimensions of 380 × 53 mm (length × diameter) and hence is able to accommodate the module with an overall constraint of 52 mm; flow through the fibers is thus in a vertical direction entering from its lower manifold. The Oxford instrument used in this work features 3D magnetic field gradients for spatial encoding; maximum gradients in the X, Z and Y directions (as defined in Fig. 2) are 27, 33 and 26 Gauss/cm, respectively. This allows for spatially resolved MR velocity imaging of flow within a module in the transverse plane (the X-Z plane) along its longitudinal direction (the Y axis). An image slice thickness of 30 mm was used that was perpendicular to the longitudinal direction of the fibers; this was located at a distance of 40 mm from the fiber's entrance manifold.

The MRI pulse sequence used for velocity imaging was the pulsed gradient spin echo, as shown in Fig. 3. A 90° soft RF pulse is accompanied by a slice-selection gradient along the longitudinal (y) direction of the fibers. Frequency encoding (G_r) and slice selection (G_s) imaging gradients are flow compensated to reduce artifacts caused by flow-related motions. The field of view was 75 mm × 75 mm and the resultant images comprised 512 × 512 voxels with an in-plane spatial resolution of 146 μm. The total acquisition time for the velocity images was 3 h. More details regarding the MRI experimental parameters used for velocity measurements are listed in Table 1.

3.4. Ultrafiltration experimental procedure

The experimental flow loop (and membrane module) used is schematically shown in Fig. 4. The UF HF module was inserted into the bore of the MRI magnet in order to perform an in-situ measurement of the flow velocity inside the individual fibers. The relevant feed solution (3 L) was pumped into the fibers using a Masterflex peristaltic pump (from Cole-Parmer), and the flow rate was maintained at 100 mL/min. A Masterflex pulse dampener was installed immediately after the pump to minimise pulsations and provide steady flow. The throttle valves were used for removing any potential air trapped inside the fibers at the beginning of each filtration and fouling experiment. Two pressure gauges (PG) were installed at the inlet and outlet of the membrane module to monitor the differential pressure. Pressure was measured using a Cerabar T PMP131 device (Endress and Hauser) and recorded using an Ecograph T Multi Channel Recorder RSG30 (Endress and Hauser).

3.4.1. Fouling experiments

Five series of fouling experiments were conducted, where each series involved the use of different foulants (as summarised in Table 2) and/or cleaning solutions. For the experiment series number #1 and #2, the feed solution contained 10 and 100 ppm of PE MPs in DI water, respectively. For the third experimental series, 1 mL of alginate gel was introduced into the system between the DI water tank (3 L) and peristaltic pump, as shown in Fig. 4. For the fourth and fifth experimental series, 1 mL of alginate gel was injected into the flowing module feed

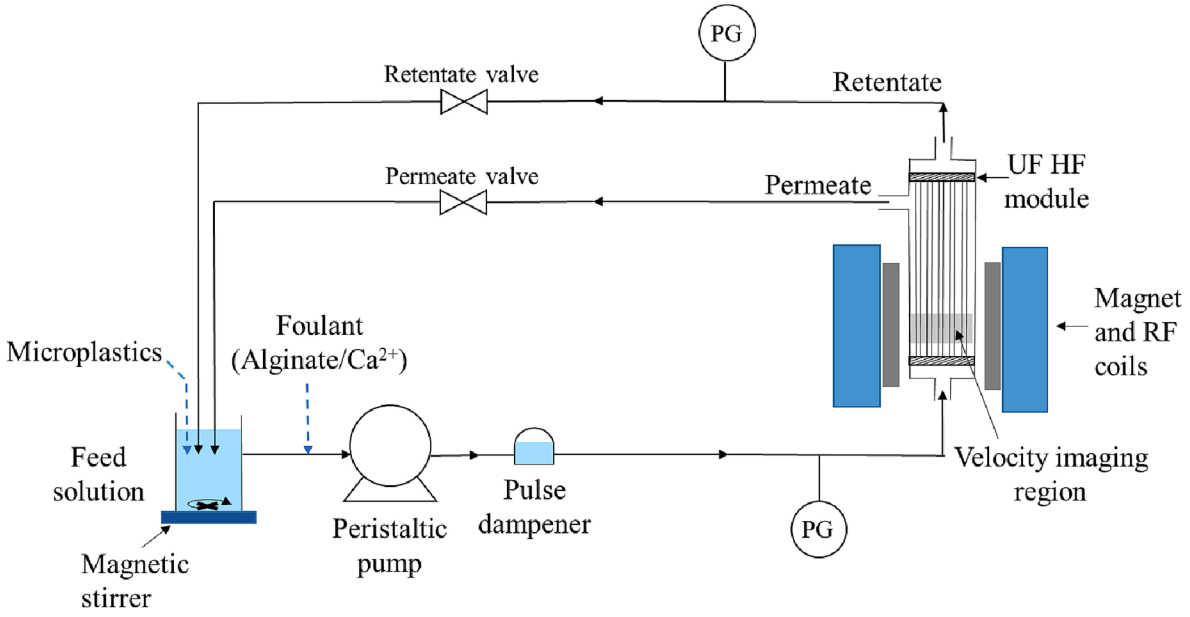

Fig. 4. Scheme of the MRI flow loop setup.

Table 2
List of foulants and their concentration used for each experiment.

Experiment series number	Foulants	
	MPs	Alginate gel
#1	10 ppm	–
#2	100 ppm	–
#3	–	6.7×10^{-5} wt%
#4	10 ppm	6.7×10^{-5} wt%
#5	100 ppm	6.7×10^{-5} wt%

solution (3 L), which contained 10 and 100 ppm PE MPs, respectively. All the feed solutions containing MPs were continuously stirred at 300 rpm using a magnetic stirrer (as shown in Fig. 4) in order to keep the MPs dispersed in the feed solution.

For the fouling experiments, both permeate and retentate flows were returned to the feed tank and recirculated for at least 24 h. For experimental series 3–5, alginate gel was injected only once at the beginning of the experimental series. The volumetric flow rate (through the fibers) was measured twice for each experimental series. The first measurement was taken before the fouling experiment using a clean membrane, and the second one was after 24 h of filtration. Velocity imaging was conducted after 30 min, 14 h and 24 h of circulation of the relevant feed solution. The membranes were flushed, backwashed, and if needed, chemically cleaned (as detailed below) after each operation before a new experimental series was commenced.

3.4.2. Hydraulic and chemical cleaning

After each fouling experiment, the next step was cleaning the fouled module, both hydraulically and using chemical cleaning. Hydraulic cleaning was conducted by flushing and backwashing (reverse flow) the membrane module with deionised water at a flow rate of 1000 mL/min for a time period of one hour. A 0.04 g/L NaOH solution (pH 11) was used for chemical cleaning of the membranes fouled with alginate. NaOH alkaline solution results in the hydrolysis and solubilisation of organic foulants and was chosen due to the organic nature of the alginate foulant [48]. Chemical cleaning was carried out by soaking the fibers in the prepared NaOH solution for five hours to allow for enough time for the solution to react with the adsorbed foulants on the membrane surface or pores. Subsequent rinsing of the fibers with deionised water was also conducted to wash off any dislodged contaminants and residual chemicals. The effectiveness of each cleaning method was assessed using MRI velocity mapping to determine the flow distribution between fibers.

3.5. Fiber detection

The acquired 512 × 512 pixel velocity images at a spatial isotropic in-plane resolution of 146 μm were analysed to determine the location of the 400 fibers. The image analysis algorithm was developed by Yan *et al.* [35] and is presented as a flowchart in Supplementary Information (Fig. S1). In summary, the image was first binary gated to identify the voxels containing flowing water, and a mask was applied to remove the peripheral space outside the HF module. Canny's edge detection [49] was then applied to detect flowing water-fiber interfaces by searching for local gradient maxima in the images of interest. Identified edge voxels were allocated a value of 1, while all other voxels were allocated a value of 0. A second masking value was then applied to remove the outer surface of the HF casing. The algorithm then proceeded by removing any isolated, unconnected edge voxels via a search space consisting of 3 × 3 pixels, which was systematically scanned across all edges containing pixels. It then searched for various circle-like shapes as constituted by the edge containing pixels; this was achieved by expanding the subspace around each edge pixel until the maximum density was determined. This process effectively identified each fiber's centre of gravity, and was hence able to detect pixels defining the fiber walls and the pixels they enclose. After a fiber was identified, it was removed from the image and the process was repeated until all fibers were identified. Individual fiber identification using the velocity image enables the quantification of volumetric flow rates through individual fibers, which allows any changes in volumetric flow rate through individual fibers to be quantified as a result of fouling and subsequent cleaning.

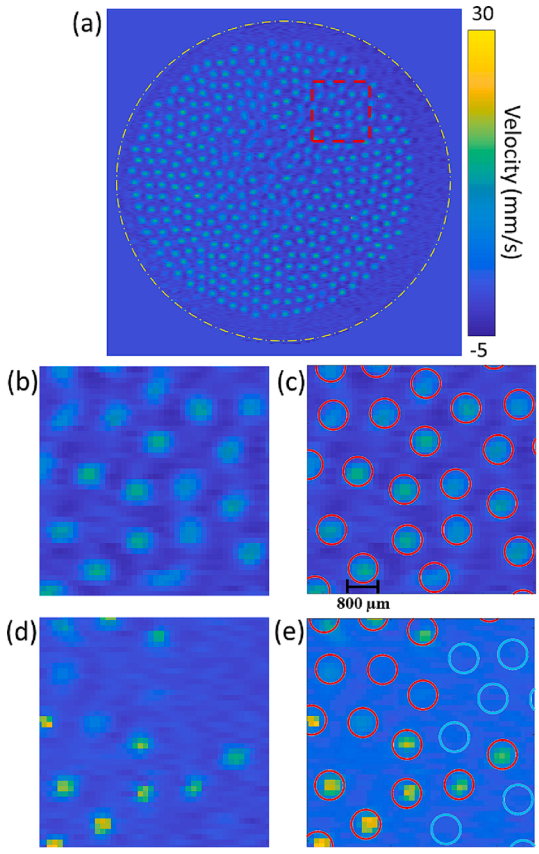

Fig. 5. (a) Velocity image of a clean fiber bundle in an operating HP module. (b) and (c) A zoomed-in region (red-dashed box in (a)) of the velocity image for a clean membrane and corresponding fiber detection. (d) and (e): The exact location equivalent zoomed-in region of a velocity image for the membrane subsequently fouled by alginate gel and the corresponding fiber detection image. A red circle is an indication of an active fiber and a blue circle is an indication of a substantially blocked or fouled fiber (defined as having a volumetric flow rate less than 10% of the mean fiber flow rate). (For interpretation of the references to colour in this figure legend, the reader is referred to the web version of this article.)

During the fouling experiments, the foulants were introduced into the system in a controlled manner, causing gradual blockage in the fibers and making their effective internal diameter smaller over time. This may eventually result in the full blockage of the fibers. As long as a fiber is not fully blocked, fluid can flow through it and the flow velocity can generally be measured using MRI. The fiber can then be identified via the fiber detection technique outlined previously. Fig. 5 shows a sample velocity images with fiber detection of the membrane samples before and after fouling. In Fig. 5(a), a sample velocity image of a clean membrane is presented – all 400 fibers can be identified. The area in the dashed box was selected to zoom in to make the individual fibers visibly clearer for the reader. Fig. 5(b) and (c) show the zoomed aforementioned region of the velocity image before fouling. Fig. 5(d) and (e) show the same region after fouling by alginate gel. Fig. 5(c) and (e) show fiber detection based on the unfouled velocity image – the location of the fibers is shown using circles. In Fig. 5, the fibers with a flow rate higher than 10% of their average fiber flow rate were allocated as 'active' fibers and are shown with a red circle in the velocity images

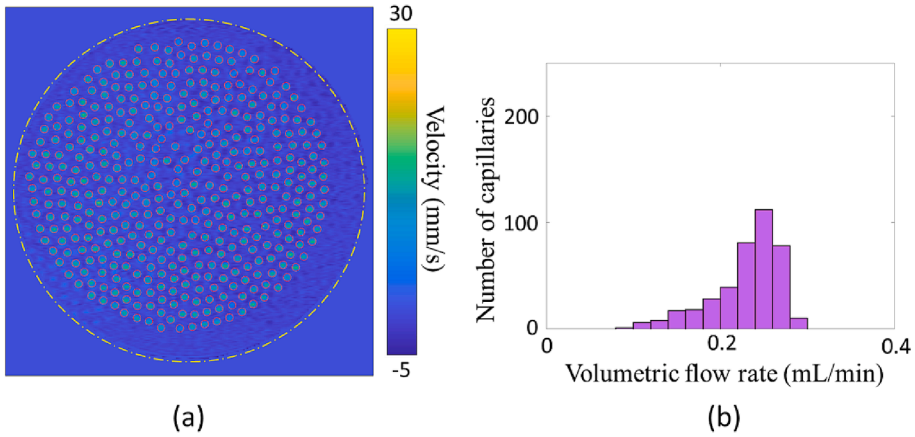

Fig. 6. (a) Fiber detection (red circles) superimposed on a velocity image of the unfouled membrane module and (b) histogram of volumetric flow rate in individual fibers. (For interpretation of the references to colour in this figure legend, the reader is referred to the web version of this article.)

whilst the substantially fouled fibers (defined as a fiber flow rate less than 10% of the average fiber flow rate) are shown using blue circles. This approach was followed for all 2D velocity images shown in this paper.

4. Results and discussion

4.1. Fouling behaviour of alginate/MPs as measured by MRI

Fig. 6(a) shows the velocity image for the unfouled membrane module with the fibers detected using the algorithm outlined above (shown using red circles); all 400 fibers were detected. This velocity image showed no significant changes over 24 h of operation (all 400 fibers continued to be detectable), hence, Fig. 6(a) can be used as a baseline for the initial location and diameter of the individual fibers within the module (when this specific module is fouled). The histogram of the number distribution of volumetric flow rate calculated in the individual fibers (The sum of the velocities in all contained pixels times the cross-sectional area of a pixel) is shown in Fig. 6(b). The minimum and maximum flow rates inside the individual fibers were 0.08 and 0.3 mL/min, respectively, with the main distribution peak located around 0.25 mL/min. This range reflects subtle variations in fiber diameter and length, their attachment to the manifolds at either rate and the attainable imaging resolution (the average fiber diameter corresponds to 5.5 pixels).

Initially, the fouling behaviour of MPs alone was investigated. PE MPs (125 μm) with concentrations of 10 and 100 ppm were dispersed in DI water and pumped through the membrane in a recirculated manner for 24 h – experimental series 1 and 2. Velocity imaging and subsequent fiber detection were then conducted. Feed solution containing 10 ppm MPs had no observable effect on the membrane and all the fibers remained active (i.e., they were the same as in Fig. 6). Fiber detection superimposed on the velocity image after recirculation of a 100 ppm MPs solution is shown in Fig. 7(a), where now 392 out of the 400 fibers remained active (did not suffer greater than 90% reduction in individual fiber flow). Thus a subtle but significant (relative to a clean feed solution) extent of fiber fouling was evident. Hydrophobic interactions between the PE particles and the membrane surface occur in water and can cause the adsorption of these particles onto the membrane surface [50]. Fouling is however limited as the hydrodynamic shear associated with cross-flow leads to ready detachment and the prevention of a significant foulant cake layer [24,51]. This was shown to be the case when the membrane was cleaned by flushing with DI water at a flow rate of 1000 mL/min for an hour. The MRI velocity image acquired after this simple hydraulic cleaning (Fig. 7(b)) showed that the flow through 100% of the 400 fibers could be 'recovered', demonstrating the reversible nature of

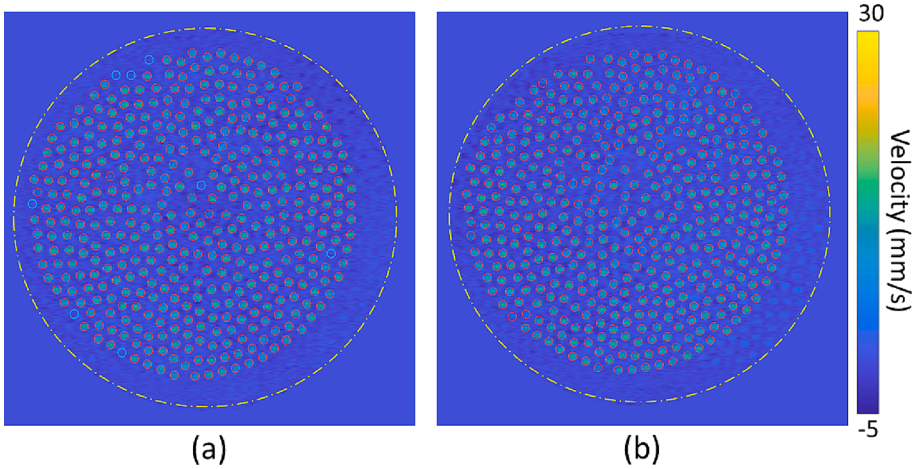

Fig. 7. Fiber detection superimposed on 2D velocity images (a) after recirculation of 100 ppm MPs solution for 24 h and (b) after hydraulic cleaning. Blue circles in (a) show fibers that are not active as a consequence of PE MP accumulation (greater than 90% reduction in fiber flow rate relative to the mean fiber flow rate). (For interpretation of the references to colour in this figure legend, the reader is referred to the web version of this article.)

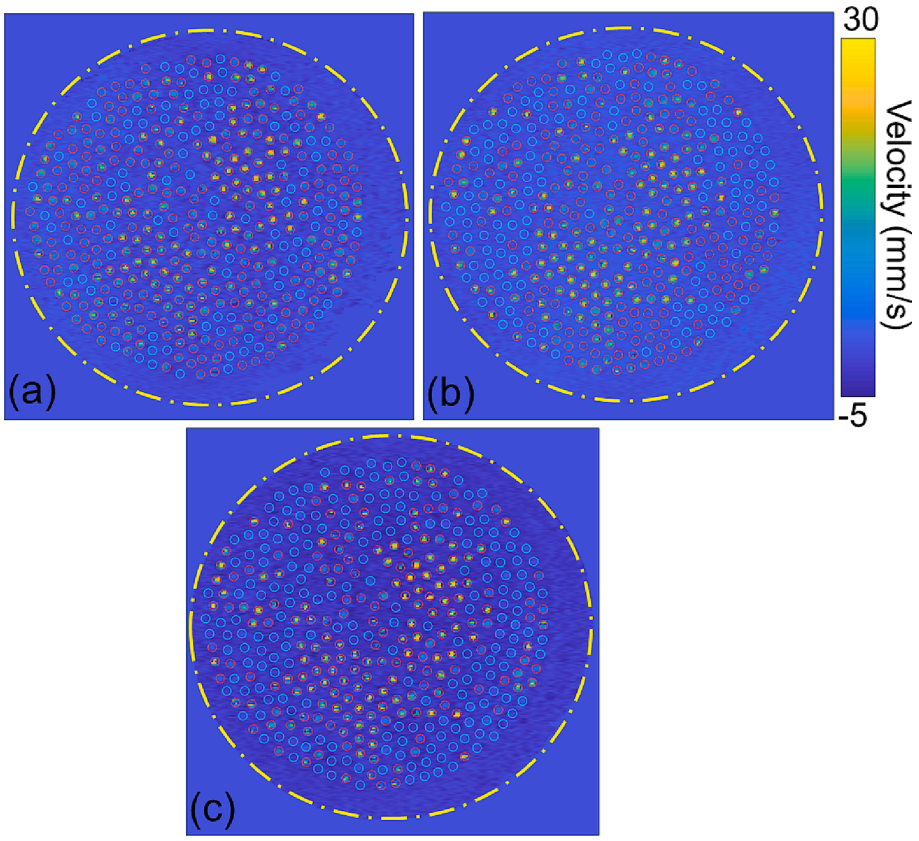

Fig. 8. Fiber detection superimposed on velocity images acquired (a) 30 min, (b) 14 h and (c) 24 h after injection of 1 mL of alginate solution to the DI water stream being fed to the module. The system operates in recirculation mode.

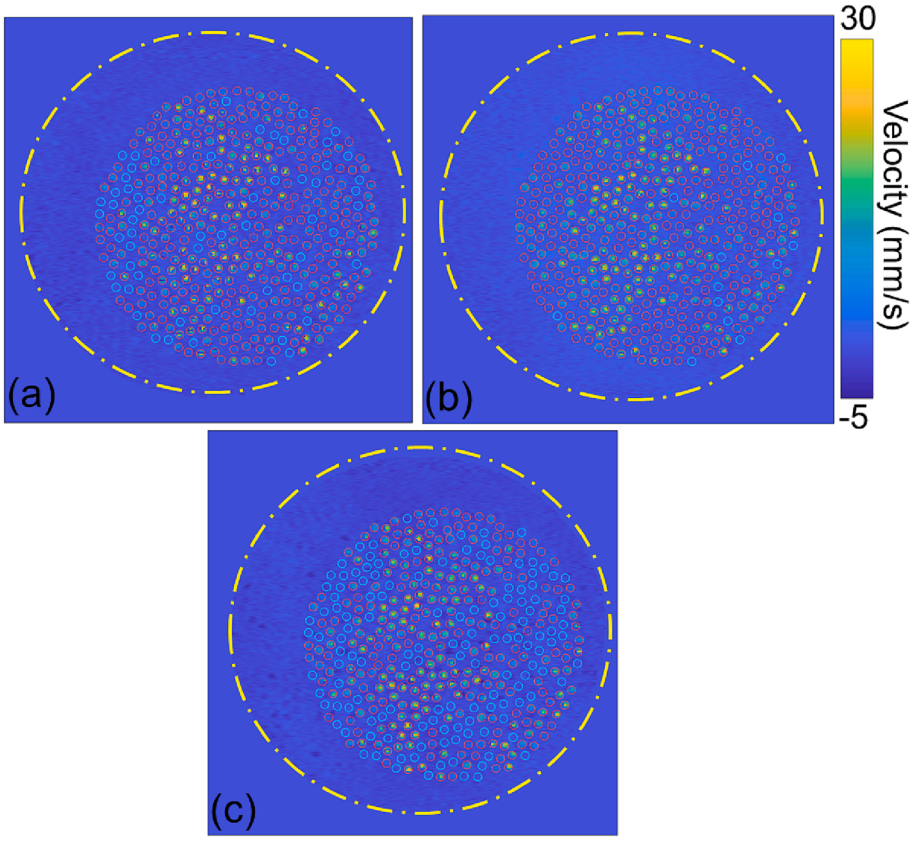

Fig. 9. Fiber detection superimposed on velocity images acquired (a) 30 min, (b) 14 h and (c) 24 h after injection of 1 mL of alginate solution and 10 ppm of MP into the DI water stream being fed to the module. The system operates in recirculation mode.

MPs fouling in this case.

In practice, wastewater effluents present variable and complex compositions, meaning that any MP fouling will highly likely not occur in isolation. These potential foulants (e.g., organics, inorganic salts, biological entities, extracellular polymeric substances) can interact with the MPs in a potentially synergistic manner, resulting in potentially more acute fouling [22]. Hence, HF membrane module fouling induced by alginate gel in the absence and presence of PE MPs at two concentrations of 10 and 100 ppm in DI water was studied (experimental series 3, 4 and 5 respectively). Fig. 8 shows velocity images (experimental series 3) indicating the impact of fouling development in the HF module by alginate gel only (in the absence of MPs) as a function of fouling time. Compared to MP fouling, the impact is much more severe. Thirty minutes after the introduction of the alginate solution, 24% of the fibers become inactive (Fig. 8(a)), this is compensated by greater volumetric flow rates in the remaining active fibers. This gradually worsened to 29% of the fibers being inactive (Fig. 8(b)) after 14 h and 49% of the fibers being inactive after 24 h (Fig. 8(c)). The impact is clearly non-linear.

The membrane module fouled with the same alginate gel solution but with the addition of 10 ppm MPs in the feed solution is presented in Fig. 9. In this case, the onset of fouling resulted in only 15% of the fibers being inactive after 30 min (Fig. 9(a)). This remained relatively unchanged after 14 h (10% inactive – Fig. 9(b)), but increased to 34% inactive after 24 h (Fig. 9(c)). The slight reduction after 14 h potentially suggests that the foulant in this case is comparatively easy to dislodge. This is admittedly indirect evidence of the formation of a more porous fouling layer in the presence of MPs but is consistent with the following literature which explores fouling development using high precision imaging but much simpler membrane geometries. In Ma *et al.* [27], MPs behaviour during coagulation and UF processes in a flat-sheet polyvinylidene fluoride (PVDF) membrane was studied. It was reported that the structure of the fouling layer formed by Fe-based coagulant alone was different from the one formed by the mixture of Fe-based coagulant and PE particles. It was observed that MPs made the cake layer more heterogeneous with larger pores, resulting in that being comparatively easier to dislodge. Chen [25] also observed that the presence of MPs can make fouling easier to dislodge.

The velocity images in Fig. 9 are more heterogeneous than those in Fig. 8 as they present substantially more fibers in which the volumetric flow rate is reduced (albeit not by 90%). This suggests the foulant formed is more porous (they don't eliminate flow, they reduce it) and hence heterogeneous. Fig. 10 shows the equivalent data when fouling occurred via the addition of the alginate solution along with 100 ppm of MPs. In this case, only 6% of the fibers were inactive after 30 min of exposure (Fig. 10(a)), this increased to 33% and 36% of fibers inactive after 14 and 24 h of exposure (Fig. 10(b) and (c), respectively). Increased heterogeneity in flow through the fibers is again evident.

Fig. 11 reproduces the velocity maps from Figs. 8 to 10 after 24 h of fouling. The numbers of active fibers in Fig. 11(a)–(c) are 203, 265 and 257, respectively. Thus, the inclusion of MPs appears to result in less severe fouling in terms of our definition of "fiber activity". In the case of MP inclusion, there are more fibers experiencing a reduction in volumetric flow rate, albeit not by 90%, so that they are considered active. The maximum velocity in an individual fiber measured for a clean membrane was 19 mm/s. This, however, increased to 32, 28 and 33 mm/s after 24 h following the introduction of the alginate gel to DI water, 10 ppm MPs solution and 100 ppm MPs solution, respectively.

Histograms of the fiber-based volumetric flow rate are shown in Fig. 12 as extracted from the three velocity images in Fig. 11. In the case of fouling with 100 ppm MPs present, more than 88% of the fibers experienced a greater than 50% reduction in velocity relative to their pre-fouled condition. This partial blockage can potentially be attributed to the comparatively porous structure of the fouling caused by the

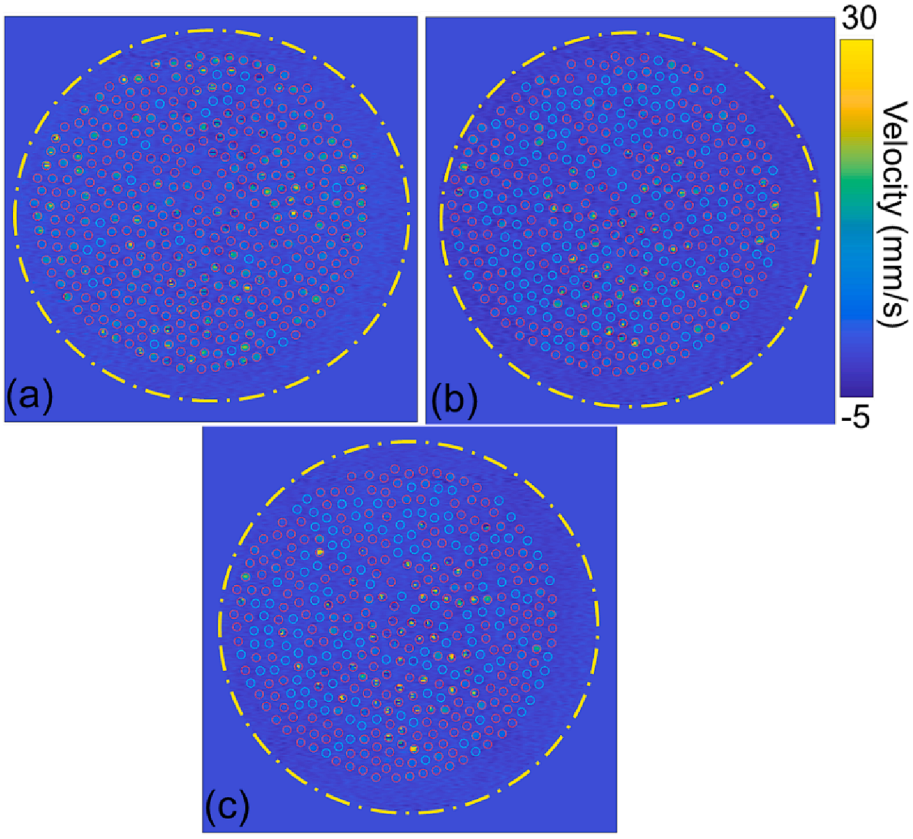

Fig. 10. Fiber detection superimposed on velocity images acquired (a) 30 min, (b) 14 h and (c) 24 h after injection of 1 mL of alginate solution and 100 ppm of MP to the DI water stream being fed to the module. The system operates in recirculation mode.

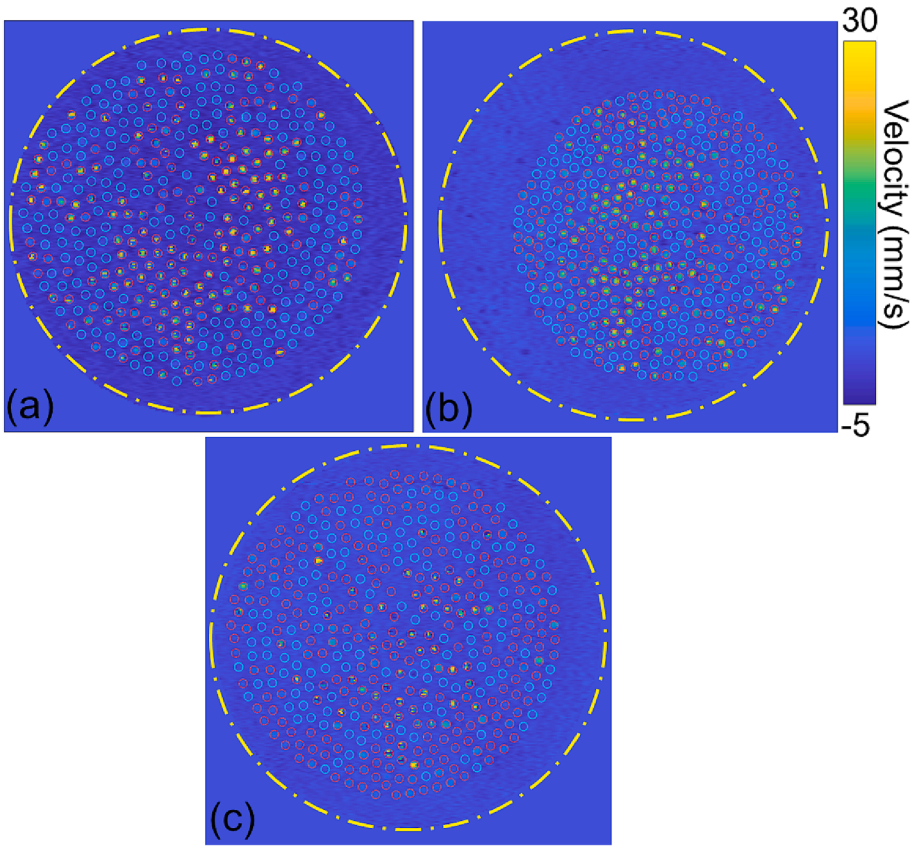

Fig. 11. Velocity images and identified fibers, 24 h after injecting 1 mL alginate gel into (a) DI water, (b) a 10 ppm MPs solution and (c) a 100 ppm MPs solution.

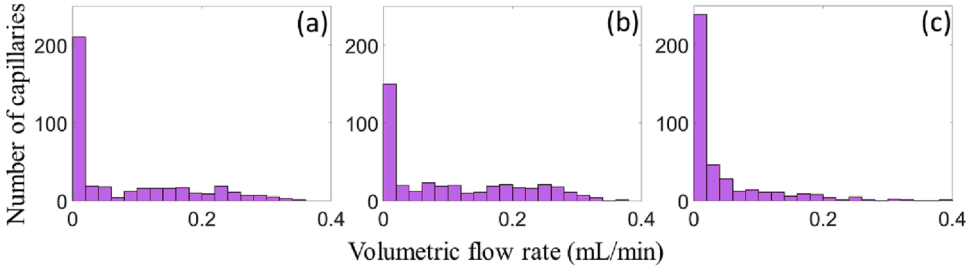

Fig. 12. Histograms of volumetric flow rate in individual fibres 24 h after injecting 1 mL alginate gel into (a) DI water, (b) 10 ppm MPs solution, (c) 100 ppm MPs solution.

presence of MPs, which still allows for some fluid transport through the respective fiber.

4.2. Permeation flow rate and differential pressure measurements

The permeation change for the different foulants is reported in Table 3. The permeate flow rate for alginate gel only was reduced by 57% (from 14 mL/min to 6 mL/min) after 24 h of filtration. Guo *et al.* [52] also reported a 58% permeation flux decline for a PVDF UF HF membrane fouled with alginate gel after 30 min of dead-end filtration. For alginate/10 ppm MPs measurement, the permeate flow rate decreased from 14 mL/min to 9 mL/min, a significantly smaller reduction than the case with no MPs present in the feed solution. The permeate flow rate only reduced to 11 mL/min for the alginate/100 ppm MPs measurement. This is all consistent with the formation of a more porous fouling layer in the presence of MPs as reported in the following literature. The impact of MPs and bacterial extracellular polymers on the forward osmosis (FO) membrane fouling was investigated by Wang *et al.*

Table 3
Permeate flow rate before and after building up the fouling layer with different foulants.

Foulant	Permeate flow rate before introducing the foulant (mL/min)	Permeate flow rate after 24 h of filtration with foulant (mL/min)
Alginate gel	14 ± 0.5[a]	6 ± 0.5 (57 %[b])
Alginate gel/ 10 ppm MPs	14 ± 0.5	9 ± 0.5 (36%)
Alginate gel/ 100 ppm MPs	14 ± 0.5	11 ± 0.5 (21%)

[a] The errors reported for flowrate represent the largest potential error in cylinder volume measurement, all measurements were performed for one minute.

[b] Values in parenthesis give the percentage permeate flow rate decline after 24 h of operation.

[26], and a similar result was found. Serious fouling happened with the feed solution containing only bacterial extracellular polymers (without MPs). The SEM image of the FO membrane surface fouled by bacterial extracellular polymers only showed a compact fouling layer, leading to a high filtration resistance and complete blockage of the pores. However, SEM images showed that, for the co-existence of bacterial extracellular polymers and MPs, the structure of the fouling layer was porous with some cracks in it that allowed the feed solution to penetrate through it, consistent with less permeation flux decline being observed. The effect of MPs accumulation on sludge floc characteristics and fouling behaviour in a PVDF membrane bioreactor was also studied by Maliwan *et al.* [18] over four months. The results showed that the presence of MPs resulted in a decrease in sludge floc size, floc hydrophobicity, and EPS molecular size, as well as an increase in EPS concentration and the floc's negative zeta potential. The combined effect of these factors resulted in a reduction of membrane fouling due to the scouring effect of the MPs on the membrane surfaces. Markazi *et al.* [20] studied the combined effect of Bovin serum albumin (BSA) and MPs on polyethersulfone UF membranes. It was observed, in agreement with Maliwan *et al.* [18] that the cake layer formed by the combined MPs/BSA foulant had a looser structure than the fouling formed by BSA alone, making it easier to dislodge. This suggests that MPs interfered with the adsorption of BSA to the membrane surface resulting in lower fouling resistance.

Table 4
Differential pressure across the modules fibers for different feed solutions.

Feed solution	Inlet P (bar)	Outlet P (bar)	ΔP (bar)
Water	0.11 ± 0.002	0.03 ± 0.001	0.08 ± 0.003
Alginate gel	0.12 ± 0.001	0.05 ± 0.001	0.07 ± 0.002
Alginate gel/10 ppm MPs	0.15 ± 0.006	0.07 ± 0.001	0.08 ± 0.007
Alginate gel/100 ppm MPs	0.14 ± 0.002	0.001	0.08 ± 0.003

The differential pressure across the fiber bundle (cross-membrane pressure drop) was also measured for all experiments – this is reported in Table 4. The differential pressure was constant at 0.07–0.08 bar during the 24 h of filtration for all the systems considered and was hence essentially invariant with time or extent of fouling. This data serves to highlight that the observed variations in system hydrodynamics and resultant permeation decline are not accessible via this bulk pressure drop characterisation.

4.3. Fouling resistance to hydraulic and chemical cleaning

Velocity imaging was conducted again after hydraulic and chemical cleaning of the modules to measure the efficiency of each cleaning method. Fig. 13(a) shows that hydraulic cleaning (backwashing) had a limited contribution to recovering all the fibers fouled by alginate gel in the absence of MPs. The number of active fibers increased from 203 (51%) to 365 (82%) after hydraulic cleaning, but the fouling could not be reduced further. To remove the residual fouling and recover the remaining fouled fibers, chemical cleaning was conducted. Fig. 13(b) shows that chemical cleaning was more effective than hydraulic cleaning for removing this residual fouling with 100% recovery of fibers to their original flow conditions. The alkaline solution used clearly broke down the chemical bonds of the residual organic foulant and made it easier to be removed [48].

Histograms of the flow rates inside the individual fibers after

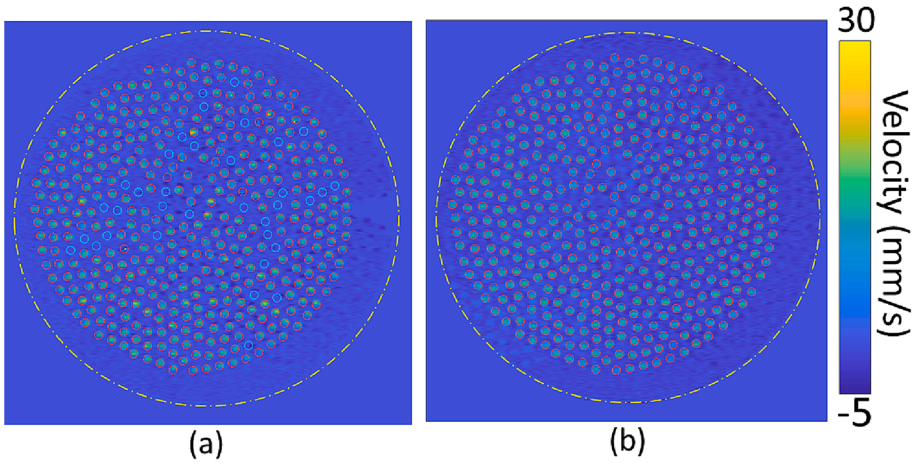

Fig. 13. Fiber detection superimposed on velocity images after (a) hydraulic cleaning and (b) subsequent chemical cleaning of alginate gel fouling (in the absence of MPs) of the HF module.

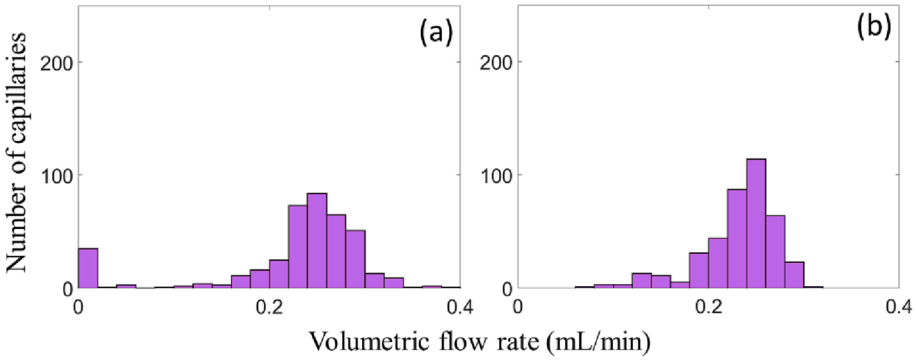

Fig. 14. Histograms of fiber flow rates (a) after hydraulic cleaning and (b) after chemical cleaning of alginate gel fouling (in the absence of MPs).

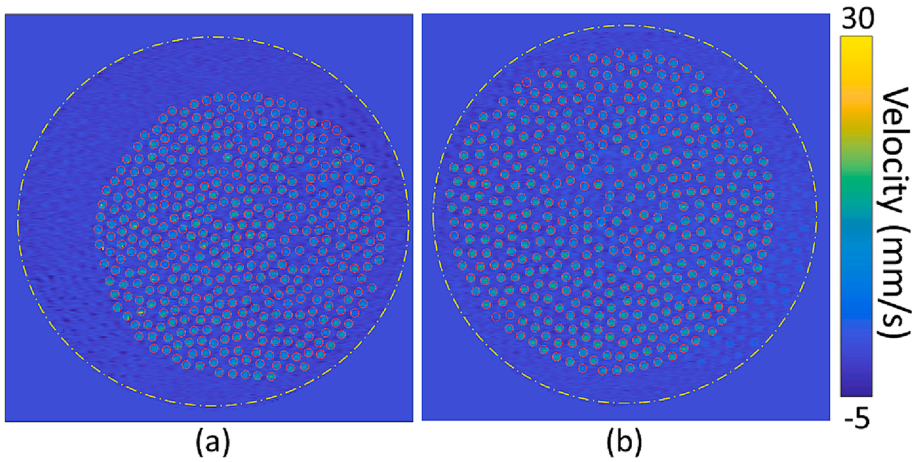

Fig. 15. Fiber detection superimposed on velocity maps after hydraulic cleaning of fouling from (a) alginate/10 ppm MPs solution (b) alginate/100 ppm MPs solution.

hydraulic and chemical cleaning are shown in Fig. 14(a) and (b), respectively. It can be observed that there are still a significant number of fouled fibers after hydraulic cleaning, leading to an increase in the flow rate in the active fibers with a detectable maximum flow rate of 0.4 mL/min. After chemical cleaning, the flow distribution resembled that of a clean module (Fig. 6(b)). The main peak shifted back to 0.25 mL/min with a lowest and highest flow rate of 0.06 and 0.32 mL/min, respectively.

Hydraulic cleaning was more efficient in removing the fouling induced by alginate gel in the presence of MPs (both 10 ppm and 100 ppm); all 400 fibers were recovered (Fig. 15(a) and (b)), meaning that chemical cleaning was superfluous. That can be attributed to the looser fouling structure formed in the presence of MPs leading to the higher efficiency of backwashing in removing the fouled layer. The lower resistance of the fouling formed by alginate gel in the presence of MPs can plausibly be attributed to porous fouling caused by the presence of PE particles.

This work has demonstrated the capability of MRI velocity mapping to quantify the co-effect of MPs and alginate gel on the fouling development inside an HF membrane module. This study focused on the impact of relatively new MPs on the membrane fouling, which has significant importance according to the constant influx of new MPs into water treatment systems [53]. However, in natural environments, MPs undergo different aging processes such as exposure to UV radiation, mechanical tensions, chemical oxidation and colonization of bacteria and other organisms on their surface. These aging processes can change the physicochemical properties of MPs, including reducing their hydrophobicity, breaking them down into smaller particles and altering their surface chemistry [54]. Consequently, aged MPs may very likely have a different impact on membrane fouling behaviour compared to 'pristine' MPs, as they can interact differently with the membrane surface and other foulants present in the feed solution [15]. Future work will focus on implementing MRI velocity mapping to study the effect of aged MPs on the membrane fouling.

5. Conclusion

Individual and combined effects of MPs and alginate gel on the fouling of a HF membrane module containing 400 parallel fibers were investigated using MRI velocity measurements. Both fouling formation and the impact of hydraulic and chemical cleaning on its reversal were thus measured in-situ on an individual fiber basis using MRI techniques. Fouling development inside the individual fibers was confirmed through a decline or loss of flow rate through individual fibers. No significant fouling was observed when only MP was used as a foulant. A compact fouling was observed when alginate gel was introduced to the DI water and recirculated inside the module which could not be backwashed and removed completely. Chemical cleaning was required in this case for full fouling remediation. The presence of MPs in the feed solution together with the alginate gel resulted in a comparatively loose, reversible fouling due to the heterogeneous and porous structure of the fouling layer caused by the presence of MPs. Due to this, the membrane modules could be fully restored by backwashing alone. We believe that the findings of this study show that in situ flow field measurement of multi-fiber HF membranes by MRI is a promising tool to monitor both the fouling development during filtration process and the efficiency of cleaning processes to recover the fibers.

Declaration of Competing Interest

The authors declare that they have no known competing financial interests or personal relationships that could have appeared to influence the work reported in this paper.

Data availability

Data will be made available on request.

Appendix A. Supplementary data

Supplementary data to this article can be found online at https://doi.org/10.1016/j.cej.2023.143320.

References

[1] B. Ma, W. Xue, C. Hu, H. Liu, J. Qu, L. Li, Characteristics of microplastic removal via coagulation and ultrafiltration during drinking water treatment, Chem. Eng. J. 359 (2019) 159–167, https://doi.org/10.1016/j.cej.2018.11.155.
[2] X. Zhang, H.-N. Li, C.-Y. Zhu, X.-J. Huang, A. Greiner, Z.-K. Xu, Biomimetic gill-inspired membranes with direct-through micropores for water remediation by efficiently removing microplastic particles, Chem. Eng. J. 434 (2022), 134758, https://doi.org/10.1016/j.cej.2022.134758.
[3] C.-L. Bai, L.-Y. Liu, Y.-B. Hu, E.Y. Zeng, Y. Guo, Microplastics: a review of analytical methods, occurrence and characteristics in food, and potential toxicities to biota, Sci. Total Environ. 806 (2022), 150263, https://doi.org/10.1016/j.scitotenv.2021.150263.
[4] M. Smith, D.C. Love, C.M. Rochman, R.A. Neff, Microplastics in seafood and the implications for human health, Curr. Environ. Health Rep. 5 (3) (2018) 375–386.
[5] R. Mercogliano, C.G. Avio, F. Regoli, A. Anastasio, G. Colavita, S. Santonicola, Occurrence of microplastics in commercial seafood under the perspective of the human food chain: a review, J. Agric. Food Chem. 68 (19) (2020) 5296–5301, https://doi.org/10.1021/acs.jafc.0c01209.
[6] C. Yuan, H. Almuhtaram, M.J. McKie, R.C. Andrews, Assessment of microplastic sampling and extraction methods for drinking waters, Chemosphere 286 (2022), 131881, https://doi.org/10.1016/j.chemosphere.2021.131881.

[7] M. Pittroff, Y.K. Müller, C.S. Witzig, M. Scheurer, F.R. Storck, N. Zumbülte, Microplastic analysis in drinking water based on fractionated filtration sampling and Raman microspectroscopy, Environ. Sci. Pollut. Res. Int. 28 (42) (2021) 59439–59451, https://doi.org/10.1007/s11356-021-12467-y.

[8] S.M. Mintenig, M.G.J. Löder, S. Primpke, G. Gerdts, Low numbers of microplastics detected in drinking water from ground water sources, Sci. Total Environ. 648 (2019) 631–635, https://doi.org/10.1016/j.scitotenv.2018.08.178.

[9] Z. Wang, T. Lin, W. Chen, Occurrence and removal of microplastics in an advanced drinking water treatment plant (ADWTP), Sci. Total Environ. 700 (2020), 134520, https://doi.org/10.1016/j.scitotenv.2019.134520.

[10] M. Pivokonsky, L. Cermakova, K. Novotna, P. Peer, T. Cajthaml, V. Janda, Occurrence of microplastics in raw and treated drinking water, Sci. Total Environ. 643 (2018) 1644–1651, https://doi.org/10.1016/j.scitotenv.2018.08.102.

[11] J. Sun, X. Dai, Q. Wang, M.C.M. van Loosdrecht, B.-J. Ni, Microplastics in wastewater treatment plants: detection, occurrence and removal, Water Res. 152 (2019) 21–37, https://doi.org/10.1016/j.watres.2018.12.050.

[12] I.A. Ricardo, E.A. Alberto, A.H. Silva Júnior, D.L.P. Macuvele, N. Padoin, C. Soares, H. Gracher Riella, M.C.V.M. Starling, A.G. Trovó, A critical review on microplastics, interaction with organic and inorganic pollutants, impacts and effectiveness of advanced oxidation processes applied for their removal from aqueous matrices, Chem. Eng. J. 424 (2021) 130282.

[13] K. Hu, W. Tian, Y. Yang, G. Nie, P. Zhou, Y. Wang, X. Duan, S. Wang, Microplastics remediation in aqueous systems: strategies and technologies, Water Res. 198 (2021), 117144, https://doi.org/10.1016/j.watres.2021.117144.

[14] M. Lee, W. Choi, G. Lim, Electrokinetic-assisted filtration for fast and highly efficient removal of microplastics from water, Chem. Eng. J. 452 (2023), 139152, https://doi.org/10.1016/j.cej.2022.139152.

[15] M. Golgoli, M. Khiadani, A. Shafieian, T.K. Sen, Y. Hartanto, M.L. Johns, M. Zargar, Microplastics fouling and interaction with polymeric membranes: a review, Chemosphere 283 (2021), 131185, https://doi.org/10.1016/j.chemosphere.2021.131185.

[16] Y. Hyeon, S. Kim, E. Ok, C. Park, A fluid imaging flow cytometry for rapid characterization and realistic evaluation of microplastic fiber transport in ceramic membranes for laundry wastewater treatment, Chem. Eng. J. 454 (2023), 140028, https://doi.org/10.1016/j.cej.2022.140028.

[17] M. Shen, T. Hu, W. Huang, B. Song, G. Zeng, Y. Zhang, Removal of microplastics from wastewater with aluminosilicate filter media and their surfactant-modified products: performance, mechanism and utilization, Chem. Eng. J. 421 (2021), 129918, https://doi.org/10.1016/j.cej.2021.129918.

[18] T. Maliwan, W. Pungrasmi, J. Lohwacharin, Effects of microplastic accumulation on floc characteristics and fouling behavior in a membrane bioreactor, J. Hazard. Mater. 411 (2021), 124991, https://doi.org/10.1016/j.jhazmat.2020.124991.

[19] L. Li, D. Liu, K. Song, Y. Zhou, Performance evaluation of MBR in treating microplastics polyvinylchloride contaminated polluted surface water, Mar. Pollut. Bull. 150 (2020), 110724, https://doi.org/10.1016/j.marpolbul.2019.110724.

[20] S. Ayoubian Markazi, M. Karimi, B. Yousefi, M. Sadati, H. Khoramshahi, S. Khoee, M.R. Karimi, Experimental and modeling study on the simultaneous fouling behavior of micro/nanoplastics and bovine serum albumin in ultrafiltration membrane separation, Journal of Environmental, Chem. Eng. 11 (2) (2023), 109354, https://doi.org/10.1016/j.jece.2023.109354.

[21] M. Golgoli, M. Khiadani, T.K. Sen, A. Razmjou, M.L. Johns, M. Zargar, Synergistic effects of microplastics and organic foulants on the performance of forward osmosis membranes, Chemosphere 311 (2023), 136906, https://doi.org/10.1016/j.chemosphere.2022.136906.

[22] X. Xiong, T. Bond, M. Saboor Siddique, W. Yu, The stimulation of microbial activity by microplastic contributes to membrane fouling in ultrafiltration, J. Membr. Sci. 635 (2021) 119477.

[23] X. Xiong, M.S. Siddique, N.J.D. Graham, W. Yu, Towards microplastics contribution for membrane biofouling and disinfection by-products precursors: the effect on microbes, J. Hazard. Mater. 426 (2022), 127797, https://doi.org/10.1016/j.jhazmat.2021.127797.

[24] J. Li, B. Wang, Z. Chen, B. Ma, J.P. Chen, Ultrafiltration membrane fouling by microplastics with raw water: Behaviors and alleviation methods, Chem. Eng. J. 410 (2021), 128174, https://doi.org/10.1016/j.cej.2020.128174.

[25] M. Chen, J. Nan, Y. Xu, J. Yao, H. Wang, X. Zu, Effect of microplastics on the physical structure of cake layer for pre-coagulated gravity-driven membrane filtration, Sep. Purif. Technol. 288 (2022), 120632, https://doi.org/10.1016/j.seppur.2022.120632.

[26] Z. Wang, K. Liu, Y. Gao, G. Li, Z. Li, Q. Wang, L. Guo, T. Liu, M.A. Al-Namazi, S. Li, Removal and fouling influence of microplastics in fertilizer driven forward osmosis for wastewater reclamation, Membranes (Basel) 11 (11) (2021), https://doi.org/10.3390/membranes11110845.

[27] B. Ma, W. Xue, Y. Ding, C. Hu, H. Liu, J. Qu, Removal characteristics of microplastics by Fe-based coagulants during drinking water treatment, J. Environ. Sci. 78 (2019) 267–275, https://doi.org/10.1016/j.jes.2018.10.006.

[28] C. Hachemi, M. Enfrin, A.O. Rashed, V. Jegatheesan, P.D. Hodgson, D.L. Callahan, J. Lee, L.F. Dumée, The impact of PET microplastic fibres on PVDF ultrafiltration performance – A short-term assessment of MP fouling in simple and complex matrices, Chemosphere 310 (2023), 136891, https://doi.org/10.1016/j.chemosphere.2022.136891.

[29] X. Yang, E.O. Fridjonsson, M.L. Johns, R. Wang, A.G. Fane, A non-invasive study of flow dynamics in membrane distillation hollow fiber modules using low-field nuclear magnetic resonance imaging (MRI), J. Membr. Sci. 451 (2014) 46–54, https://doi.org/10.1016/j.memsci.2013.09.015.

[30] S.-E. Wu, Y.-C. Lin, K.-J. Hwang, T.-W. Cheng, K.-L. Tung, High-efficiency hollow fiber arrangement design to enhance filtration performance by CFD simulation, Chem. Eng. Process. – Process Intesif. 125 (2018) 87–96, https://doi.org/10.1016/j.cep.2018.01.003.

[31] X. Xu, Y. Jian, Y. Xue, Q. Hou, L. Wang, Microplastics in the wastewater treatment plants (WWTPs): occurrence and removal, Chemosphere 235 (2019) 1089–1096, https://doi.org/10.1016/j.chemosphere.2019.06.197.

[32] M. Enfrin, J. Lee, P. Le-Clech, L.F. Dumée, Kinetic and mechanistic aspects of ultrafiltration membrane fouling by nano- and microplastics, J. Membr. Sci. 601 (2020), 117890, https://doi.org/10.1016/j.memsci.2020.117890.

[33] N. Schork, S. Schuhmann, H. Nirschl, G. Guthausen, Compressed sensing MRI to characterize sodium alginate deposits during cross-flow filtration in membranes with a helical ridge, J. Membr. Sci. 626 (2021), 119170, https://doi.org/10.1016/j.memsci.2021.119170.

[34] F. Arndt, S. Schuhmann, G. Guthausen, S. Schütz, H. Nirschl, In situ visualization of flow and fouling layer formation in ceramic hollow fiber membranes by magnetic resonance imaging (MRI), 2016.

[35] B. Yan, N.W. Bristow, S.J. Vogt, J.S. Vrouwenvelder, M.L. Johns, E.O. Fridjonsson, Monitoring of hollow fiber module velocity field and fouling inside individual fibers using benchtop MRI, J. Membr. Sci. 629 (2021), 119238, https://doi.org/10.1016/j.memsci.2021.119238.

[36] L.T. Yogarathinam, J. Usman, M.H.D. Othman, A.F. Ismail, P.S. Goh, A. Gangasalam, M.R. Adam, Low-cost silica based ceramic supported thin film composite hollow fiber membrane from guinea corn husk ash for efficient removal of microplastic from aqueous solution, J. Hazard. Mater. 424 (2022), 127298, https://doi.org/10.1016/j.jhazmat.2021.127298.

[37] S.A. Creber, J.S. Vrouwenvelder, M.C.M. van Loosdrecht, M.L. Johns, Chemical cleaning of biofouling in reverse osmosis membranes evaluated using magnetic resonance imaging, J. Membr. Sci. 362 (1) (2010) 202–210, https://doi.org/10.1016/j.memsci.2010.06.052.

[38] E.O. Fridjonsson, S.J. Vogt, J.S. Vrouwenvelder, M.L. Johns, Early non-destructive biofouling detection in spiral wound RO membranes using a mobile earth's field NMR, J. Membr. Sci. 489 (2015) 227–236, https://doi.org/10.1016/j.memsci.2015.03.088.

[39] X. Li, Y. Mo, J. Li, W. Guo, H.H. Ngo, In-situ monitoring techniques for membrane fouling and local filtration characteristics in hollow fiber membrane processes: a critical review, J. Membr. Sci. 528 (2017) 187–200, https://doi.org/10.1016/j.memsci.2017.01.030.

[40] N.W. Bristow, S.J. Vogt, K.T. O'Neill, J.S. Vrouwenvelder, M.L. Johns, E. O. Fridjonsson, Flow field in fouling spiral wound reverse osmosis membrane modules using MRI velocimetry, Desalination 491 (2020), 114508, https://doi.org/10.1016/j.desal.2020.114508.

[41] M. Zargar, R. Ujihara, S.J. Vogt, J.S. Vrouwenvelder, E.O. Fridjonsson, M.L. Johns, Imaging of membrane concentration polarization by NaCl using 23Na nuclear magnetic resonance, J. Membr. Sci. 600 (2020), 117868, https://doi.org/10.1016/j.memsci.2020.117868.

[42] S. Schuhmann, J.W. Simkins, N. Schork, S.L. Codd, J.D. Seymour, M. Heijnen, F. Saravia, H. Horn, H. Nirschl, G. Guthausen, Characterization and quantification of structure and flow in multichannel polymer membranes by MRI, J. Membr. Sci. 570–571 (2019) 472–480, https://doi.org/10.1016/j.memsci.2018.10.072.

[43] F. Arndt, U. Roth, H. Nirschl, S. Schütz, G. Guthausen, New insights into sodium alginate fouling of ceramic hollow fiber membranes by NMR imaging, AIChE J. 62 (7) (2016) 2459–2467, https://doi.org/10.1002/aic.15226.

[44] F. Arndt, S. Schuhmann, G. Guthausen, S. Schütz, H. Nirschl, In situ MRI of alginate fouling and flow in ceramic hollow fiber membranes, J. Membr. Sci. 524 (2017) 691–699, https://doi.org/10.1016/j.memsci.2016.11.079.

[45] N. Schork, S. Schuhmann, F. Arndt, S. Schütz, G. Guthausen, H. Nirschl, MRI investigations of filtration: Fouling and cleaning processes, Microporous Mesoporous Mater. 269 (2018) 60–64, https://doi.org/10.1016/j.micromeso.2017.05.042.

[46] J.W. Simkins, S. Schuhmann, G. Guthausen, M. Heijnen, S.L. Codd, J.D. Seymour, Characterization of biofilm distribution in hollow fiber membranes using compressed sensing magnetic resonance imaging, J. Membr. Sci. 594 (2020), 117437, https://doi.org/10.1016/j.memsci.2019.117437.

[47] M. Wiese, O. Nir, D. Wypysek, L. Pokern, M. Wessling, Fouling minimization at membranes having a 3D surface topology with microgels as soft model colloids, J. Membr. Sci. 569 (2019) 7–16, https://doi.org/10.1016/j.memsci.2018.09.058.

[48] M. Jafari, A. D'Haese, J. Zlopasa, E.R. Cornelissen, J.S. Vrouwenvelder, K. Verbeken, A. Verliefde, M.C.M. van Loosdrecht, C. Picioreanu, A comparison between chemical cleaning efficiency in lab-scale and full-scale reverse osmosis membranes: role of extracellular polymeric substances (EPS), J. Membr. Sci. 609 (2020), 118189, https://doi.org/10.1016/j.memsci.2020.118189.

[49] J. Canny, A computational approach to edge detection, IEEE Transactions on pattern analysis and machine intelligence (6) (1986) 679–698.

[50] S.H. Joo, Y. Liang, M. Kim, J. Byun, H. Choi, Microplastics with adsorbed contaminants: mechanisms and treatment, Environ. Challenges 3 (2021), 100042, https://doi.org/10.1016/j.envc.2021.100042.

[51] Q. Li, Z. Wang, C. Liu, X. Wang, A new combined cake-complete model with the cake resistance corrected by cake filtration equilibrium coefficient in cross-flow microfiltration, J. Environ. Chem. Eng. 10 (1) (2022), 106956, https://doi.org/10.1016/j.jece.2021.106956.

[52] X. Guo, X. Chen, W. Hu, Studies on cleaning the polyvinylchloride ultrafiltration membrane fouled by sodium alginate, Environ. Technol. 30 (5) (2009) 431–435, https://doi.org/10.1080/09593330902757454.
[53] S.H. Akyildiz, R. Bellopede, H. Sezgin, I. Yalcin-Enis, B. Yalcin, S. Fiore, Detection and analysis of microfibers and microplastics in wastewater from a textile company, Microplastics 1 (4) (2022) 572–586.
[54] H. Luo, Y. Zhao, Y. Li, Y. Xiang, D. He, X. Pan, Aging of microplastics affects their surface properties, thermal decomposition, additives leaching and interactions in simulated fluids, Sci. Total Environ. 714 (2020), 136862, https://doi.org/10.1016/j.scitotenv.2020.136862.
[55] B. Yan, B. Blankert, S. J. Vogt, J. S. Vrouwenvelder, M. L. Johns and E. O. Fridjonsson, Monitoring residual fouling after cleaning of multi-fiber membrane modules fiber-by-fiber using non-invasive MRI monitoring, Water Research 2023 Vol. 229 Pages 119384 DOI: https://doi.org/10.1016/j.watres.2022.119384.